RML Glove—An Exoskeleton Glove Mechanism With Haptics Feedback

Zhou MA, *Student Member, IEEE*, and Pinhas Ben-Tzvi, *Senior Member, IEEE*

Abstract—**This paper presents the design, implementation, and experimental validation of a haptic glove mechanism: the RML glove (Robotics and Mechatronics Lab). The designed haptic interface is a lightweight, portable, and self-contained mechatronic system that fits on a bare hand and provides haptic force feedback to each finger of the hand without constraining their movement. In order to experimentally test the new design, teleportation with this glove for mobile robot navigation is also studied. By comparing teleportation experiments with and without force feedback, the results show that this new admittance (using force as input and position as output) glove with force feedback can provide effective force feedback to the user and augment telepresence.**

Index Terms—**Exoskeleton, force feedback, haptic interface, teleoperation mapping.**

I. INTRODUCTION

HAPTIC interfaces can measure one's body position and movement, while concurrently providing operators with touch, force or torque information generated from a remote or virtual environment [1]. During the last decade, haptic devices have been utilized in many applications for medical training and rehabilitation [2], [3], telesurgery [4], [5], telenavigation [6]–[9], as well as micromanipulation [10], [11].

As one type of haptic devices, haptic gloves expand the capabilities of force feedback by allowing the user to feel virtual objects in a much more natural way. This ability is required in many applications [12]. The high dexterity of haptic gloves also makes them applicable to the control of complex movements of remote robots, as opposed to other haptic devices such as joysticks and PHANTOM [13]. Although many research activities have been performed on haptic glove designs [14]–[23], they either restrict the natural motion and maximum output force of the hand or are bulky and heavy.

Turner *et al.* completed tests for a commercial haptic glove known as the CyberGrasp [14]. The CyberGrasp is a haptic device with one-direction active force feedback, which fits on the hand, and provides force feedback to each finger [15]. In order to reduce the weight and size of the mechanism, the glove joints

were activated by a cable-driven mechanism which transmits the force between the fingers and a distant Actuator Unit. With this design the load of the haptic device was reduced on the hand, but the outside Actuator Unit still restricted the natural motion of the hand to 1 m spherical radius from the Actuator Unit due to limited cable length [15]. Also, the one-direction activation mechanism limits its application.

Blake *et al.* employed magneto-rheological brakes (MR brakes) to develop a haptic glove referred to as the MR glove, with a wearable size placed on the back of the fingers [16]. Passive force was transmitted through small MR brakes connected directly to the exoskeleton links instead of using cables. MR brakes can apply passive torque up to 899 Nm·m on three fingers in both flexion and extension directions. However, the entire glove weighed 640 g; the load concentrated on the fingers and creates a discomfort to the operator when using the glove for an extended period of time. Besides, an MR brake requires high current drivers and high capacity batteries, which are bulky and heavy. Moreover, the MR glove which employs controllable brakes belongs to the category of passive haptic devices [1] that cannot provide active force feedback to the operator. The ability to create an active feedback can be quite useful to increase the flow of information between the device and the user. Without active force feedback, there is no energy exchanged between the device and the user as a function of the feedback control, and the user's hand will not perceive kinesthetic information of a manipulated object, such as position or movement.

On the other hand, the Rutger Master II (Bouzit *et al.* [17]) was developed using four custom pneumatic actuators arranged inside the palm of the hand. The objective of the mechanism was to deliver a compact and light-weight structure on the hand. The Rutger Master weighed 185 g including the wires and pneumatic tubing (excluding pneumatic actuator, power source, etc.), and provided relatively large forces up to 16 N on each of the four fingers in both flexion and extension directions. Despite its lightweight, the Rutger Master limits the hand work envelope and prevents a complete fist closure due to the placement of the actuators in the palm.

From the above analysis, the main challenges associated with haptic glove design could be summarized as follows: 1) size and weight—to be small enough to fit on human hands and to be as light as possible for portability on a hand; 2) flexibility of mechanism—to give adequate dexterity without constraining hand motions; 3) dynamic range—to be versatile enough to be used in both very sensitive activities and in large force situations.

In order to tackle all these challenges, the proposed glove mechanism is designed, integrated, and tested. This glove is lightweight and comfortable to wear and operate, providing high

Fig. 1.   Schematic of the teleoperation system.

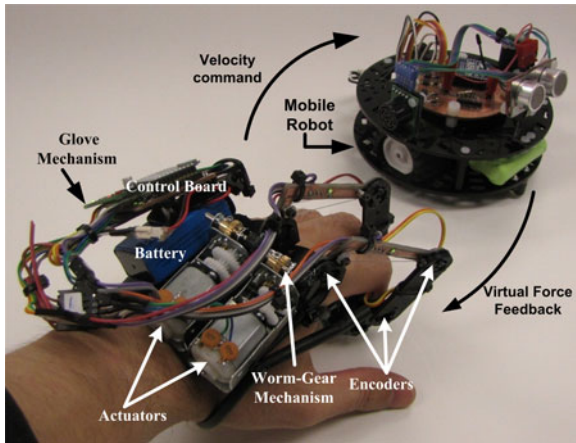

Fig. 2.   Cable transmission model.

maximum output force feedback without constraining the finger motions. Thus, the glove is a bidirectional teleoperation admittance haptic device that augments traditional control interfaces including keyboards, joysticks, and PHANTOM.

In this paper, the design, implementation, and experimental validation of the haptic glove are presented. As one possible application, teleportation with this glove for mobile robot navigation is also studied. The paper is organized as follows. Section II describes the mechanical design and modeling of the glove mechanism. Section III describes the electrical design of the system. Section IV describes the glove mechanism control system. Section V highlights the numerical and experimental validation of the mechanics model and control system, and Section VI summarizes the paper and describes future work.

II. SYSTEM LAYOUT AND MECHANICAL DESIGN

Fig. 1 shows the glove mechanism and the teleoperation experimental system analyzed in this research. Through the glove, hand gesture of the user is measured, mapped, and transmitted to the mobile robot in the form of velocity commands through a wireless network. Conversely, distance information of the objects around the robot is collected, processed, and sent back to the glove to generate a virtual interaction force to the user. Based on the feedback of this virtual force, the user can "feel" the approach to an obstacle and hence control the robot more smoothly and safely in an intuitive way with natural motions of the finger [24].

The glove prototype fits on a bare hand and is attached to the index and middle fingers at the finger tips as shown in Fig. 1. The total weight of the two-finger prototype is 180 g, including one 9-V rechargeable battery (20 g), control unit (25 g), two worm-gear actuator assemblies (35 g each), and mechanical skeleton (50 g). Because all necessary components are light and contained inside the glove, the user can move each finger freely without being tethered or feeling fatigue.

A. Actuation System

The mechanical design of each haptic glove finger consists of three main parts: three-link exoskeleton, an actuator unit, and
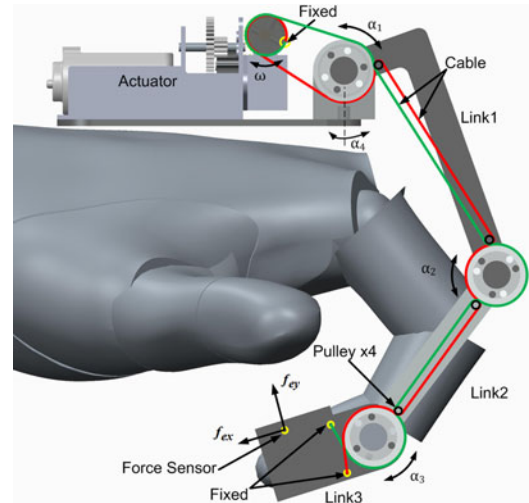
two actuation cables, as shown in Fig. 2. In order to lighten and simplify the whole glove, the movements of the Distal Interphalangeal (DIP), Metacarpophalangeal (MCP), and Proximal Interphalangeal (PIP) joints of each finger are coupled together with one actuator module. The actuator unit consists of a brushed dc-motor (Mabuchi FA-130, [25]) geared to a pulley through nonbackdrivable worm gears. The maximum speed of the actuator module is 150 r/min when powered with 9-V battery. At this speed, the time of the hand's maneuver, from fully open to close, then back to open again, is about 1 s.

Two steel cables are attached to the pulley and routed along the exoskeleton to the fingertip. Cable transmission is chosen because it can provide adequate power through narrow pathways and allow the actuator to be located away from the dexterous fingers. In addition, cables are compact, light-weight, and cost-effective and simplify the transmission. Because a cable can only be pulled for n degrees of freedom (DOF), $2n$ cables are necessary. A two-cable pull–pull transmission is used, actuated with a dc-motor located at the back of the palm. The force is exerted in both directions for extension and flexion, thereby driving the links to follow or resist finger movement. Bidirectional force control is enabled by antagonistically actuating the two cables, transferring this force along the exoskeleton to the finger tip. As shown in Fig. 2, when the actuator rotates the active pulley clockwise, the red cable is tensioned and the mechanism and the index finger close. When the actuator rotates counterclockwise, the green cable is tensioned and the finger will open.

In general, a haptic system with a real force-feedback should be capable of delivering a maximum force that matches the human hand output force. According to [26], the maximum thumb/finger strength is 35 N (male sustained hold). The designed wearable haptic device was developed to accomplish this objective in a wearable, light-weight, and compact glove system. Due to the nonbackdrivable worm gears actuator unit, this actuator is self-locking without power consumption, making the passive force as high as 35 N. The maximum active output force that the glove can provide on the finger tip is 10 N,

Finger Name	Length (mm)
Index Finger	72.0
Middle Finger	79.5
Ring Finger	75.0
Little Finger	60.5

which is slightly smaller than the commercial force-feedback glove, CyberGrasp (12 N maximum output force) [12]. But it is sufficient to provide realistic active force feedback and will not harm the operator's finger.

One extreme but commonly used condition is examined here. When the haptic device is used to touch or feel some hard object (e.g., a concrete wall), most of the motor-actuated haptic devices would make the motor run at a stalled-current mode to provide the realistic high force feedback. Due to the current/power limit of haptic devices, this "high" force is still not high enough [10]–[16] compared to the human finger output force (35 N). For the proposed glove mechanism in this situation, the motor current is zero by virtue of the self-locking characteristic of a worm-gear mechanism. Because such high force feedback only occurs in passive force output mode, the glove will not hurt or damage the fingers of the operator. With the closed-loop force-feedback control, this haptic glove could provide almost real feeling of both hard and soft materials to the operator (e.g., a concrete wall or soft cotton).

The size and shape of human fingers may vary significantly between individuals and different fingers for each person (e.g., the length of middle finger and the little finger vary. Table I shows the lengths of the author's fingers). To avoid custom designing a glove for each person and each finger, it is desirable to accommodate a large number of different people for a given design. Because each articulated linkage mechanism remains extendable when each finger is fully stretched, the same finger mechanism can easily adapt to different finger sizes. After performing several wear tests, the glove mechanism was able to adapt to each of over ten users' hands whose finger sizes ranged from 60 to 89 mm.

Fig. 3(a) and (b) illustrates the side view of a hand with the glove in stretched and bent positions. The top view in normal and abduction position is shown in Fig. 3(c) and (d). The bottom view is shown in Fig. 3(e).

Consider the mechanism in which the friction in the pulleys is neglected. When the mechanism is in static equilibrium, if there is an external force $\mathbf{f_e} = [f_{ex}, f_{ey}]^T$ applied on the tip of the finger mechanism, by virtue of the principle of virtual work, the actuators' forces $\mathbf{f_{ai}}, i = 1, 2$ (for two fingers) should be

$$\mathbf{f_a} = -J^T \mathbf{f_e} \qquad (1)$$

where J represents the Jacobian matrix of the haptic device.

According to [26], the normal force on the finger pad is more important for haptic devices. Therefore, the primary force that will be sensed by each finger in the glove will be the normal force applied to the surface of the fingertip. The accuracy of the
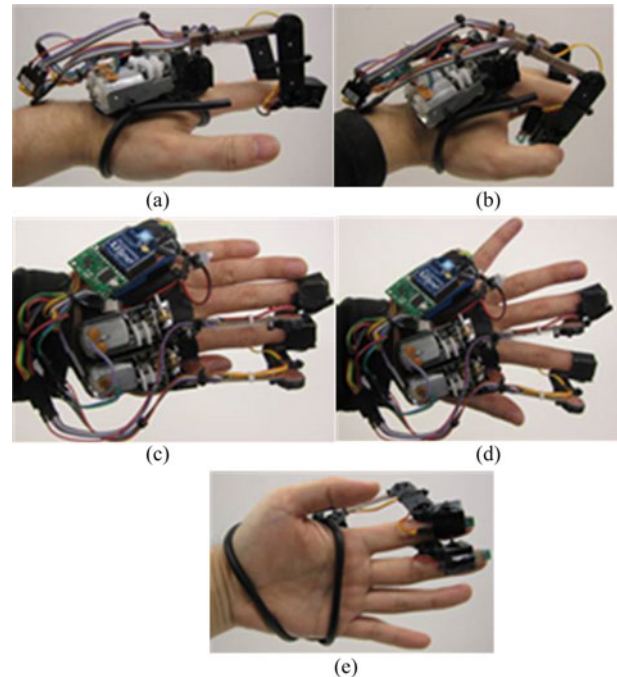

Fig. 3. Different views of the glove mechanism in stretched, bent and abduction position. (a) Side view in stretched position, (b) side view in bent position, (c) top view in stretched position, (d) top view in abduction position, (e) bottom view in stretched position.

magnitude of this normal force f_{ey}, as shown in Fig. 2, is a key factor in haptic glove and precision teleoperation grasping tasks applications. Thus, the contact force component in the other direction (i.e., f_{ex}) is ignored.

B. Kinematic Analysis

All the joints in the design were realized through revolute pin connections. Extension/flexion and adduction/abduction movements are possible with this mechanism. For each finger, the haptic mechanism and the finger itself can be modeled as one six-bar mechanism, as shown in Fig. 4(a), where the palm is taken as the ground link. Each finger consists of three links and the haptic mechanism for each finger has three links as well.

It should be noted that both the end link of the mechanism and the fingertip are fixed together, so they are considered as one link. Therefore, there are six links in total (i.e., one ground link, three finger links, and two haptic mechanism links) and six revolute pin connections (ignoring the adduction/abduction). According to Gruebler's formula, the mobility of the mechanism can be calculated

$$F = 3(n - 1) - 2f_1 - f_2 = 3 \qquad (2)$$

where F is the total DOF, n is the number of links, f_1 is the number of lower-pair DOF (one DOF), and f_2 is the number of higher-pair DOFs (two DOF). In this case, $n = 6$, $f_1 = 6$, and $f_2 = 0$. This results in a three DOF mechanism for each finger.
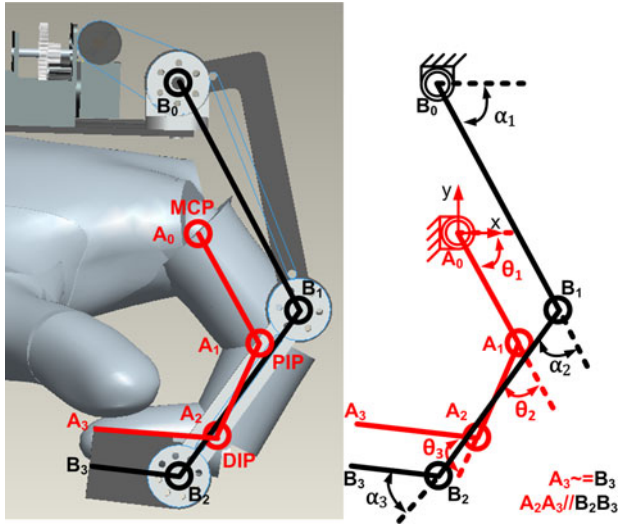
Fig. 4. Haptic glove mechanism analysis: (a) side view of a finger with the mechanism, (b) kinematic diagram showing degrees of freedom.

Based on Fig. 4, the following equations can be derived:

$$\alpha_1 = \theta_1 + \theta_2 + \theta_3 - \alpha_2 - \alpha_3 \tag{3}$$

$$x_{B_0} + \overline{B_0 B_1} \cos \alpha_1 + \overline{B_1 B_2} \cos(\alpha_1 + \alpha_2) + \overline{B_2 B_3} \cos(\alpha_1 + \alpha_2 + \alpha_3)$$
$$= \overline{A_0 A_1} \cos \theta_1 + \overline{A_1 A_2} \cos(\theta_1 + \theta_2) + \overline{A_2 A_3} \cos(\theta_1 + \theta_2 + \theta_3) \tag{4}$$

$$y_{B_0} + \overline{B_0 B_1} \sin \alpha_1 + \overline{B_1 B_2} \sin(\alpha_1 + \alpha_2) + \overline{B_2 B_3} \sin(\alpha_1 + \alpha_2 + \alpha_3)$$
$$= \overline{A_0 A_1} \sin \theta_1 + \overline{A_1 A_2} \sin(\theta_1 + \theta_2) + \overline{A_2 A_3} \sin(\theta_1 + \theta_2 + \theta_3) \tag{5}$$

where

$\overline{B_{i-1} B_i}$ length of ith mechanism link;
$\overline{A_{i-1} A_i}$ length of ith finger link;
α_i joint angle of the ith mechanism link;
θ_i joint angle of the ith finger link.

After solving (3)–(5), θ_1, θ_2, and θ_3 can be obtained as follows:

$$\theta_1 = \arctan \frac{N}{M} + \arccos \frac{p_1^2 + p_2^2 + N^2 - M^2}{2 p_1 \sqrt{M^2 + N^2}} \tag{6}$$

$$\theta_2 = \arccos \frac{M^2 + N^2 - p_1^2 - p_2^2}{2 p_1 p_2} \tag{7}$$

$$\theta_3 = \alpha_1 + \alpha_2 + \alpha_3 - \theta_1 - \theta_2 \tag{8}$$

where

$$M = x_{B_0} + \overline{B_0 B_1} \cos \alpha_1 + \overline{B_1 B_2} \cos(\alpha_1 + \alpha_2)$$
$$+ \overline{B_2 B_3} \cos(\alpha_1 + \alpha_2 + \alpha_3) - \overline{A_2 A_3} \cos(\theta_1 + \theta_2 + \theta_3)$$
$$N = y_{B_0} + \overline{B_0 B_1} \sin \alpha_1 + \overline{B_1 B_2} \sin(\alpha_1 + \alpha_2)$$
$$+ \overline{B_2 B_3} \sin(\alpha_1 + \alpha_2 + \alpha_3) - \overline{A_2 A_3} \sin(\theta_1 + \theta_2 + \theta_3)$$
$$p_1 = \overline{A_0 A_1}, \; p_2 = \overline{A_1 A_2}.$$

Equation (6)–(8) illustrate that if the joint angles for the three links of the mechanism $(\alpha_1, \alpha_2, \alpha_3)$ are known, the microcon-

TABLE II
FINGER JOINT MOTION RANGES (MEASURED FROM THE AUTHOR'S INDEX FINGER)

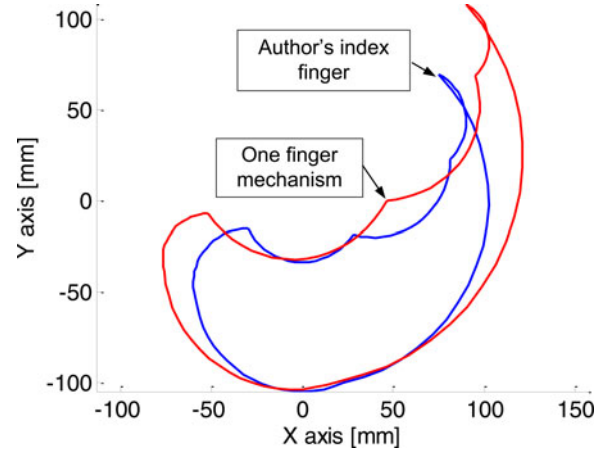| Finger Joint	Angular Motion Range (Degrees)
MCP	[-30, 90]
PIP	[-15, 90]
DIP	[-15, 90]

Fig. 5. Two-dimensional workspace for index finger and the glove mechanism.

troller can calculate the exact finger position which can be used for the control of the mobile robot.

C. Index Finger Workspace

In haptics research, one major challenge is that the human operator's motion should not be restricted by the haptic device when there is no contact with a remote or virtual object. Moreover, there should be no limit for the operator to make desired motions while operating the haptic device. Thus, adequate degrees of freedom and sufficient workspace are required for the haptic devices, especially for the haptic glove worn on the operator's hand—the most dexterous body part of the human. A multilink mechanism is chosen because it is more suitable for multiple finger inputs and has a larger workspace. According to this six-linkage mechanism model and the finger joint motion ranges as depicted in Table II, the 2-D workspace for one finger can be obtained, as shown in Fig. 5 (for $l_1 = 45$ mm, $l_2 = 30$ mm, $l_3 = 30$ mm). In a similar way, the workspace of the glove mechanism is also plotted in the same figure. As illustrated in Fig. 5, the new mechanism design can ideally cover most of the finger's workspace. In other words, the glove links allow full flexion and extension in all joints. The workspace of different finger lengths is also similar to this one.

III. ELECTRICAL DESIGN

The haptic system is composed of a glove skeleton and a control interface. The overall electrical design of the system is illustrated in Fig. 6. The interface uses a MEGA168 (Atmel Corp) microcontroller to read force sensor data, control the force magnitude applied at the user's fingertips through controlling the motor rotation, and communicate with the robot and/or host
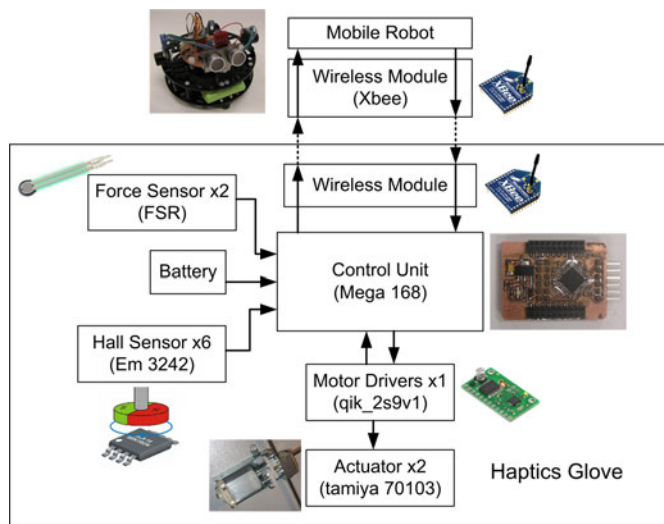
Fig. 6.   Electrical design diagram.

PC. Force sensitive resistor (FSR) sensors were used to measure normal forces, which are mounted on the finger tip pad as shown in Fig. 2. Motor current is also measured through a shunt circuit. Thus, both joint angle and torque/force measurements are required for feedback control and for data collection.

To minimize the thickness of the mechanical construction between the fingers and maximize the finger workspace, two customized printed circuit boards (PCB) with mounted three angular position encoders (Hall element sensor EM-3242) are used as the two links of the finger mechanism. Two angular position encoders that are mounted on Link 1 and one encoder on Link 3 provide accurate joint angles measurement for calculating each finger's status and position. These encoders are soldered directly onto the PCB board, which is used as both a mechanical link and a carrier of electrical components and signals. This dual function makes the glove mechanism lighter without sacrificing strength. Link 2 is made of thermoplastic and connects Links 1 and 3 through revolute pin joints.

Thus, no extra angular encoder sensors are needed to be attached to the joint. The thickest part of the glove between the fingers is merely 6 mm.

Unlike other haptic devices mentioned in the first section, which require more power input when higher force/torque is needed, the proposed glove consumes much less power due to the use of worm-gear mechanism, especially when high force feedback is required. Thus, a small capacity battery is chosen that lasts over 1 h for continuous operation and reduces the glove's weight.

Communication between the haptic glove and the mobile robot or the host computer is accomplished through wireless RF XBee modules (1-mW transmission power at 2.4 GHz provides 30-m working range indoors). The adoption of the RF module made the glove wireless, portable, and self-contained. The wireless transmission speed is 115 200 bits/s. The transmitted data from the haptic glove contain finger joint angles, measured finger tip contact forces, and input pulley speed commands for the mobile robot. The data that the haptic glove receives include

robot speed and forces to be applied to the operator's finger, which are based on the virtual spring-damper force model described in Section IV.

Additionally, software running on the microcontroller conditions the force signals and rotation sensors signals with low-pass filters. Since humans are sensitive to high-frequency information, the loop of the control program runs at 1.3 kHz, which is in excess of the typical 1 kHz recommended for haptic devices [28]. This high cycle frequency not only provides a realistic touch feeling to the haptic glove user, but also helps to maintain the stability of the whole system and provide precise output force. The communication update rate between the robot and the glove is 50 Hz.

The experimental mobile robot (Fig. 1) incorporates two brushed dc motors/encoders at the base. Differential drive control is used to navigate the robot, with the two wheels rotating together to translate and in opposition to turn. Two additional caster wheels are incorporated to balance the robot. The motor encoders are used for both closed-loop velocity control and position estimation.

When considering objects detection around the robot, sonar has the advantages of small size and low data processing complexity compared to laser sensors or stereo cameras. Due to the size and low computation power of the robot platform the authors chose, sonar sensors were sufficient. Three ultrasonic sensors (SRF08 and two SRF02 by Devantech Ltd. [29]) were mounted on the experimental mobile robot. Sonar sensors were chosen due to their low cost, ease of use, and reliability even in some complex environments, such as darkness, heavy dust or underwater. With a low-pass filter, the accuracy of the sonar can be quite acceptable. Moreover, sonar data are easily convertible to virtual force since sonar data can be considered to have a magnitude and direction as a force vector does. The experiments in Section V-E validate the sonar's performance and its reliability.

IV. CONTROL SYSTEM

A. Teleoperated Control

The teleoperation control system consists of the glove mechanism and a mobile robot as shown in Fig. 7. When the operator wears and operates the glove, the rotation angle and the status of the mechanism links are measured and each finger position is calculated via inverse kinematics solution of the mechanism (6)–(8). According to the operator's finger position and contact force, the control unit calculates the corresponding command, and sends it via wireless module to control the position and orientation of the mobile robot. When the robot receives the command, it controls the speed of the two wheels accordingly. Meanwhile, the robot converts the obstacles distance information based on ultrasonic sensors data into the form of a virtual force and sends it back to the haptic glove, which generates force feedback to the operator to represent the robot's proximity to obstacles.

When the glove is powered ON, force feedback can be provided based on the proportion of the velocity between the finger's motion and that of the worm-gear mechanism. When the glove is powered OFF, each worm-gear mechanism becomes
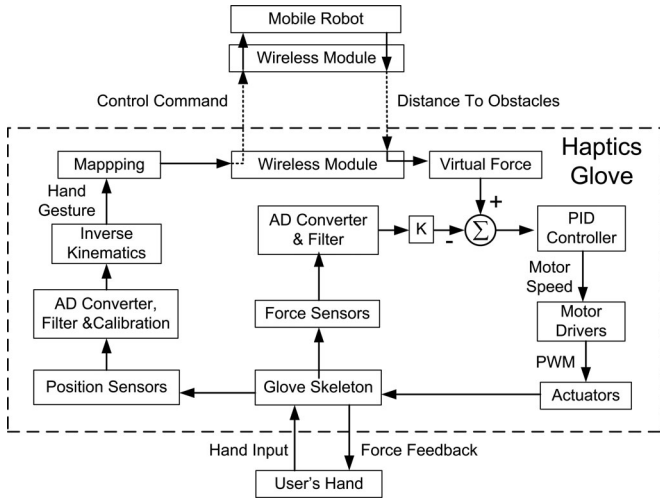
Fig. 7.   Control scheme of the teleoperation system.

nonbackdrivable. The objective of the controller is to convert the obstacles distance information from the mobile robot into an equivalent force applied at the fingertips of the operator, while compensating for the static friction of the device.

When the robot is moving fast toward or getting close to an obstacle, the haptic glove will provide a large force feedback and make it difficult for the operator to maintain the original finger position, thus it will help reduce the speed or change the direction of the robot to prevent collision. Therefore, the operator can acquire the environmental information using force feedback and control the robot in a more intuitive way.

Two different modes were developed to implement this haptic system for different applications:

1) *Human Computer Interface (HCI) mode*: where the glove works as a computer peripheral device and executes the commands from the computer to provide force feedback to the user. Due to the large number of tasks operating systems process, most computers are not suitable for real-time applications. The computer is thus chosen to be the master while the glove is the slave in the HCI mode. This feature is particularly useful when dexterous manipulation in virtual reality simulation, medical training, or rehabilitation is involved.

2) *Human Robot Interface (HRI) mode:* where the glove is used to control a mobile robot. In HRI mode, the glove is the master device and the robot is the slave. Due to the dedicated program used in this system, the glove could interact in real-time with mobile robots or other slave devices.

Under both HCI and HRI modes, configuration of variable parameters could be changed through wireless communication, such as object stiffness (maximum output force varies from 1 to 10 N), device address (for cases when two or more gloves are used), and timeout value (varies from 1 to 50 ms).

B. Model of the Mobile Robot

As shown in Fig. 8, the position (linear, angular) of the mobile robot is represented as $\mathbf{p} = [x, y, \theta]^T$.
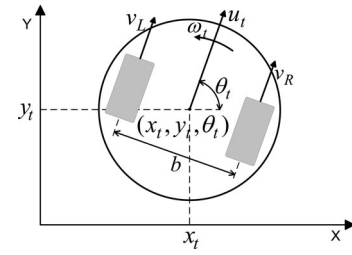

Fig. 8.   Mobile robot model.

The kinematic motion of the mobile robot can be described by

$$u = \frac{(v_R + v_L)}{2} \tag{9}$$

$$\omega = \frac{(v_R - v_L)}{b} \tag{10}$$

$$\begin{bmatrix} \dot{x} \\ \dot{y} \\ \dot{\theta} \end{bmatrix} = \begin{bmatrix} \cos\theta & 0 \\ \sin\theta & 0 \\ 0 & 1 \end{bmatrix} \begin{bmatrix} u \\ \omega \end{bmatrix} \tag{11}$$

$$\begin{bmatrix} x \\ y \\ \theta \end{bmatrix} = \begin{bmatrix} x_0 + \frac{u}{\omega}\left[\sin(\theta_0 + \omega\Delta t) - \sin(\theta_0)\right] \\ y_0 - \frac{u}{\omega}\left[\cos(\theta_0 + \omega\Delta t) - \cos(\theta_0)\right] \\ \theta_0 + \omega\Delta t \end{bmatrix} \tag{12}$$

where u and ω are linear velocity and angular velocity of the robot around its center axis, respectively; v_L, v_R are left and right wheel's velocity; b is the lateral distance between the wheels; $[x_0, y_0, \theta_0]^T$ are the position and orientation in the previous time step; Δt is the time interval between each calculation time step.

The equations given above can be used for dead reckoning by substituting v_R, v_L for the sensor data obtained from the encoder and the time value t, then solving for the values x, y and θ, and plotting the trajectory of the robot.

C. Mapping of Teleoperation

Hand gestures are extensively used in the literature for control of mobile robots [30]–[33]. In this paper, the operator's fingers' position was measured through the glove mechanism and converted to velocity commands that were transmitted to the mobile robot. The mapping between the robot velocity commands and the fingers' position is defined by (13), (14), and shown in Fig. 9

$$v_R = \begin{cases} 0, & \text{if } 30° \geq \theta_{1\text{middle}} \geq 0° \\ -k_m\theta_{1\text{middle}}, & \text{otherwise} \end{cases} \tag{13}$$

$$v_L = \begin{cases} 0, & \text{if } 30° \geq \theta_{1\text{index}} \geq 0° \\ -k_m\theta_{1\text{index}}, & \text{otherwise} \end{cases} \tag{14}$$

where k_m is the coefficient factor of mapping, $\theta_{1\text{index}}$ and $\theta_{1\text{middle}}$ are the angles of MCP joints for index and middle finger separately.
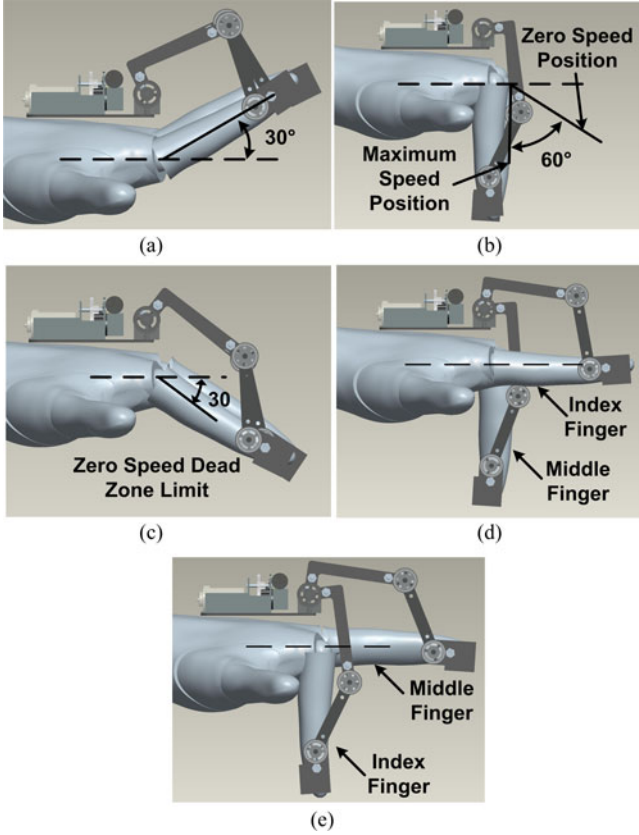
Fig. 9. Mapping between the robot velocity and the fingers position. (a) Move backward. (b) Move forward. (c) Stop. (d) Turn left. (e) Turn right.

TABLE III
MAPPING BETWEEN THE GLOVE AND THE MOBILE ROBOT

Finger Position (I:Index, M:Middle)	Locomotion of the Robot
Both [-90,-30)	Move Forward
Both [-30,0]	Stop
Both (0,30]	Move Backward
I: [-30,30], M:[-90,-30]	Turn Left
I: [-90,-30], M:[-30,3 0]	Turn Right

The index finger controls the left wheel velocity and the middle finger controls the right one. This principle of operation came from a method of using a smartphone to control a rolling ball. When the phone is tilted left, the ball turns left, and when it is tilted in the forward direction, the ball moves forward.

In order to control the robot in a simple manner, a small area in the center of the workspace called the dead zone [Fig. 9(c)] sends zero velocity commands when the finger is inside it [34]. As the finger moves outside the dead zone, the desired direction and velocity is inferred from the displacement of the mechanism from the center of the workspace (Fig. 9(a), (b) and Table III). The further out of the dead zone the mechanism is, the faster the robot will move.

The hand gestures are designed to be effective and intuitive, so that first time users can operate the robot easily with very minimal training.
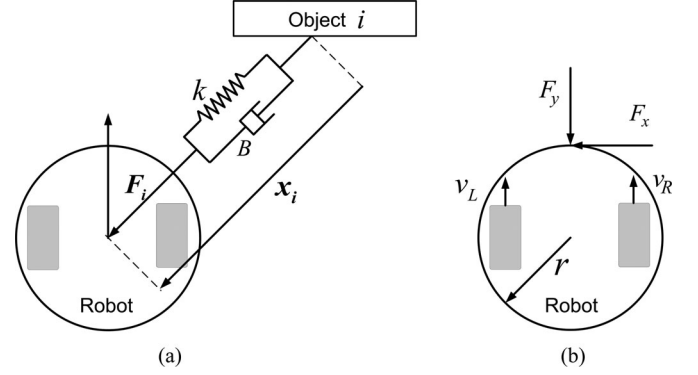

Fig. 10. Force model.

D. Force Model

Data acquired by three sonar sensors are filtered and processed to generate a virtual interaction force. Based on the robot's geometric configuration, each virtual force is computed using the following virtual spring-damper model as shown in Fig. 10(a):

$$\mathbf{F}_i = \begin{cases} k(\rho/\|\mathbf{x}_i\| - 1)\mathbf{x}_i - B\dot{\mathbf{x}}_i, & \text{when } \|\mathbf{x}_i\| < \rho \\ 0, & \text{otherwise} \end{cases} \quad (15)$$

where k is the stiffness of the virtual spring and ρ is the maximum distance of influence. It means if the distance between obstacles and the robot is larger than ρ, obstacles do not exert any repulsive force and they are not perceived by the operator. B is the damper coefficient of the virtual force model. $\dot{\mathbf{x}}_i$ is the relative velocity between the robot and the obstacles. When the robot and the objects are getting closer to each other, the damper model adds an extra force to the static spring force to prevent collision. Thus, this virtual force model is calculated to incorporate both static and dynamic obstacles.

The virtual force is calculated to incorporate all the obstacles around the robot

$$\mathbf{F} = \sum_{i=1}^{n} \mathbf{F}_i. \quad (16)$$

By projecting $\mathbf{F}$ onto the X and Y axes in the robot local coordinate system, components of force F_x and F_y can be obtained as shown in Fig. 10(b). Then, it is proposed that the virtual force F_x only affects angular velocity $\omega(F_x = I\dot{\omega}/r)$, and F_y only influences the robot's linear velocity $u(F_y = m\dot{u}$, i.e., when $F_x = 0$, the virtual force $\mathbf{F}$ only affects the linear velocity of the robot, and the angular velocity remains constant). These relations can be represented as

$$u = u_0 + \dot{u}\Delta t = u_0 + \frac{F_y}{m}\Delta t \quad (17)$$

$$\omega = \omega_0 + \dot{\omega}\Delta t = \omega_0 + \frac{F_x \cdot r}{I}\Delta t \quad (18)$$

where m and I are mass and moment of inertia (about the center axis) of the robot, respectively; r is the length of lever arm which connects the center of the robot to the application point of virtual force F_x.
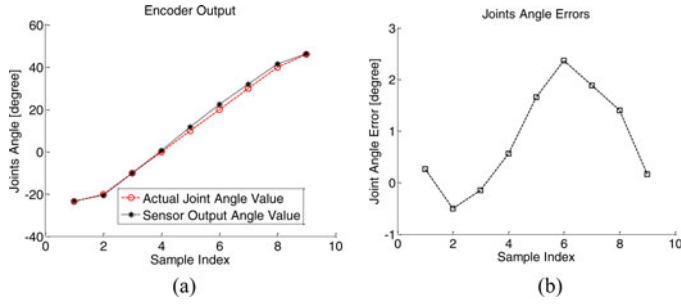
Fig. 11.   Hall-effect position sensor test. (a) Hall-effect sensor output. (b) Hall-effect sensor accuracy error.

The virtual forces applied on the right and left wheels are defined as F_R and F_L. Similar to (17), we have

$$v_R = v_{R0} + \frac{F_R}{m}\Delta t \qquad (19)$$

$$v_L = v_{L0} + \frac{F_L}{m}\Delta t \qquad (20)$$

where $v_{R0} = u_0 + \frac{\omega_0 b}{2}$ and $v_{L0} = u_0 - \frac{\omega_0 b}{2}$.

The next step is to find the relation between $\begin{bmatrix} F_x \\ F_y \end{bmatrix}$ and $\begin{bmatrix} F_R \\ F_L \end{bmatrix}$. According to (9), (10), and (17)–(20), such relations were obtained as

$$\begin{bmatrix} F_R \\ F_L \end{bmatrix} = \begin{bmatrix} \dfrac{mrb}{2I} & 1 \\ -\dfrac{mrb}{2I} & 1 \end{bmatrix} \begin{bmatrix} F_x \\ F_y \end{bmatrix}. \qquad (21)$$

The calculated virtual forces F_R and F_L are sent wirelessly from the robot to the haptic glove, which then applies those forces on the operator's two fingers separately to represent the proximity. As discussed in the previous section, the index finger controls the left wheel, thus the virtual force F_L is applied to the index finger accordingly (f_{ey} in (1)). Correspondingly, F_R is applied on the middle finger. In this scope of discussion, the robot is consistently controlled to avoid objects and does not have specific final destination, hence the virtual forces are always in the direction of extension, which means F_R and F_L are always larger than zero. It is worth mentioning that the glove mechanism is not limited to this type of application because it can generate both active and passive bidirectional forces.

Thus, when the operator bends his/her fingers to move the robot toward an object, as they are getting closer, the virtual forces applied on the operator's fingers become larger accordingly. Under the effect of these forces, the operator extends the fingers to reduce the speed of the robot and try to turn or move backward. As a result, collision between the robot and the object could be avoided.

In order to make the glove safe and practical to use, when the finger position is above the dead zone ($\theta_1 < 30°$ as shown in Fig. 11), the virtual force becomes zero. In other words, when the robot stops or moves backward, the user does not feel the virtual force.
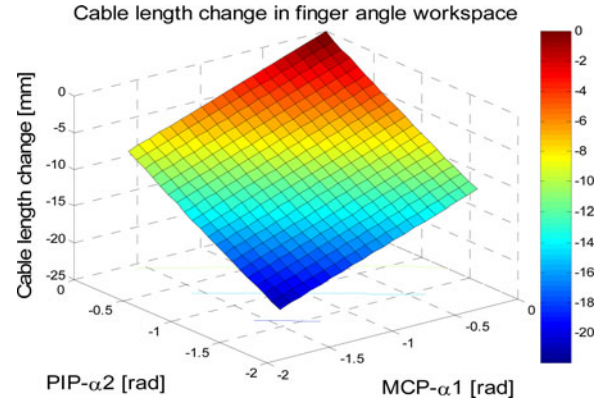

Fig. 12.   Cable length change in finger angle workspace.
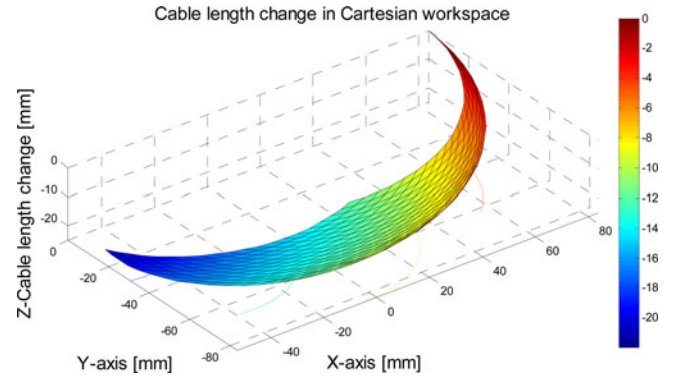

Fig. 13.   Cable length change in Cartesian workspace.

V. SIMULATION AND EXPERIMENTAL RESULTS

A. Hall-Effect Position Sensor Test

The joint rotation resolution of the hall-effect rotation sensor was experimentally tested at $0.4°$, which is the minimum rotation angle the sensor can detect. The Hall-effect rotation sensor was calibrated with a 12-bit absolute encoder (resolution: $0.088°$). The plotting of encoder output and the angle error is shown in Fig. 11(a) and (b), respectively. The actual joint values were obtained by using a 12-bit absolute encoder. The hall-effect sensor accuracy was less than $2.5°$ due to mechanical assembly vibration. The joint angle error was less than 4% of the total range of motion.

B. Simulation of Cable Length Change

Based on Fig. 2, the cable length can be derived through the following expression:

$$l = k + (\alpha_1 + \alpha_2 + \alpha_3) \cdot D \qquad (22)$$

where k is a constant that can be calculated through the geometry of the mechanism, D is the diameter of each of the three pulleys.

From (22) and (3)–(8), the cable length can be plotted when the MCP and PIP joints of the operator's fingers are changing, as shown in Figs. 12 and 13. These two figures illustrate the cable length change in both joint angle workspace and Cartesian workspace. From these two figures, it can be concluded that the cable length change is a monotonic function with respect to the
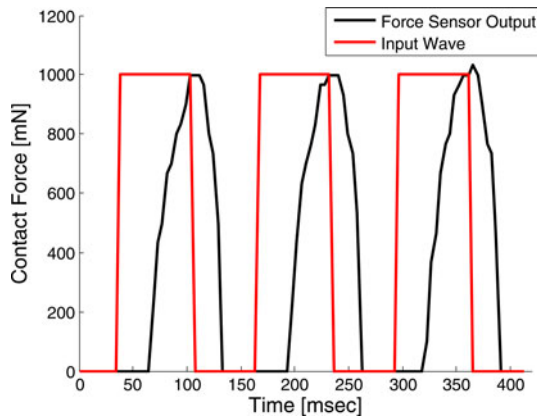
Fig. 14. Step response of the haptic glove.

angle changes. In other words, the cable length keeps increasing during the flexion of the finger and vice versa.

C. Mechanical Bandwidth

To evaluate the response speed of the prototype, the mechanical bandwidth was tested with regards to step input excitations. A PID controller was chosen (as shown in Fig. 7) to compensate for the external force applied by the operator against the virtual force and to guarantee zero error at a steady state. The PID parameters were tuned by means of a standard Ziegler–Nichols method.

As shown in Fig. 14, the glove has a good response time to a 7.5-Hz step signal. From this step response result, it can be seen that there is a roughly 30 ms time delay in the force output. The delay is mainly caused by the backlash of the worm gear.

D. Free Motion Experiment

Free motion is considered as a fundamental behavior of the haptic device. In such case, the operator should be able to move his/her fingers freely without feeling the friction and the inertia induced by the glove. The friction of the device should be eliminated via real-time control to enable free motion with zero force input from the robot. An experiment that evaluates this free motion was established to demonstrate the effectiveness of friction compensation in the control algorithm.

In this experiment, the operator wears the two-finger prototype and moves the index and middle fingers freely. The experiment consists of three open/close maneuvers in 3 s with the results shown in Fig. 15. At this speed, the maximum force that the operator could feel is less than 200 mN, which implies that the control algorithm compensated for the mechanism's internal friction successfully. Fig. 16 shows the hall-effect sensors output from the middle finger mechanism in the three maneuvers. Figs. 15 and 16 show that the contact force exhibit higher values during the flexion of the finger.

E. Mobile Robot Control

As shown in Fig. 17, experiments were set up to evaluate the performance improvement provided by the haptic glove in HRI mode. The trial area (approximately 1×1.4 m) was surrounded
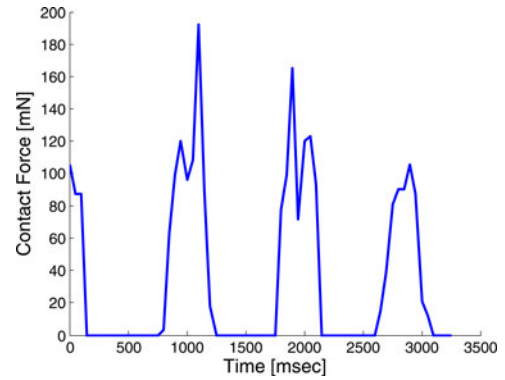

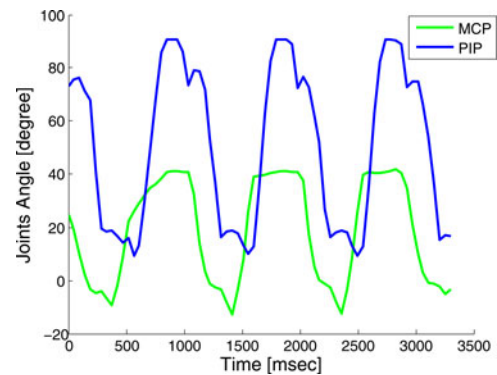Fig. 15. Contact force output in free motion experiment.

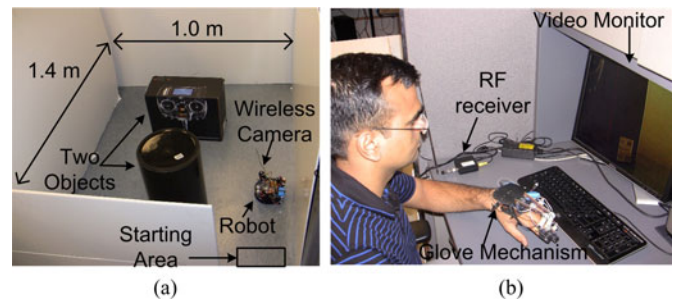Fig. 16. Joint angles of middle finger in free motion experiment.

Fig. 17. Experimental setup. (a) Trial area setup. (b) Subject using the haptic glove.

by four large white boards [Fig. 17(a)]. Two boxes (rectangular: L37 × W17 × H28 cm, cylinder: D25 × H37 cm) were located inside the enclosure. The operator's goal was to navigate the robot (D13 × H10 cm) to follow the wall and return to its start point, while avoiding collision with the objects and completing the task as quickly as possible. Initially, the robot was located inside the starting area and the angle between its translation axis and the right wall was arbitrary selected from $-30°$ to $30°$. Direct view of the trial area was obscured during the teleoperation, but the wireless camera mounted on the robot provided a real-time active view on a monitor directly in front of the glove user as shown in Fig. 17(b). Once the robot returned to the home position, the trial timing was terminated. A group of eight volunteers were asked to perform the experiment. After wearing the glove, each user was asked to work with the system for
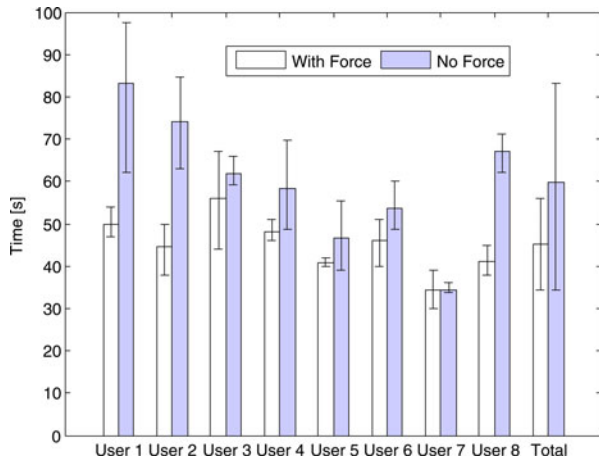
Fig. 18.　Average teleoperation time with and without force feedback.

Fig. 19.　Trajectory of the mobile robot in a navigation task with force feedback.

Fig. 20.　Force values during the navigation task. (a) Index finger force. (b) Middle finger force.

about 5 min to get used to it. Although the finger sizes of all users varied significantly (60–89 mm), the differences of α_1 were small and the control algorithm worked for all without any change of the parameters.

In the same environment, two different kinds of teleoperation experiments, without and with force feedback, were tested to drive the mobile robot to the goal position. In the first kind of the experiment, the side screws of the worm-gear mechanism were removed in order to disable the force feedback. The operator could only control the mobile robot through visual feedback on the monitor. In the second experiment, in addition to the video feedback, the force feedback function was enabled for teleoperation. All users were asked to run each experiment for three times and the completion time was recorded. For each user, the order of the experiments with and without force was randomized.

As a result, with force feedback enabled, the average task completion time ($M = 45.1$ s, $SD = 6.6$ s) was shorter than the case without force feedback ($M = 59.9$ s, $SD = 15.4$ s). The glove notably improved the task completion times ($t(8) = 4.49, p < 0.05$). The experiments showed that the glove reduced the task completion time by an average 24.7% as shown in Fig. 18.

During the no force experiment, the authors found that visual feedback alone often led to incorrect depth estimation for the user, as reported by other researchers [35], [36]. Due to the lack of correct depth information and the limited view angle, most subjects made the robot turn earlier than expected and collided with the object, especially in the first and second corners around the rectangular box. Lack of depth perception is considered the main reason for increased time in trials with no force feedback.

Since the communication between the master glove and the mobile robot was wireless, it was quite easy to use another wireless module to record all the sensors' data during each experiment for further analysis. One example of such recording with force feedback enabled is shown in Figs. 19 and 20. The map (Fig. 19) was built based on the three sonars' and two encoders' data from the robot: the red line is the robot trajectory, while the blue dots represent the obstacles. Fig. 20 illustrates the
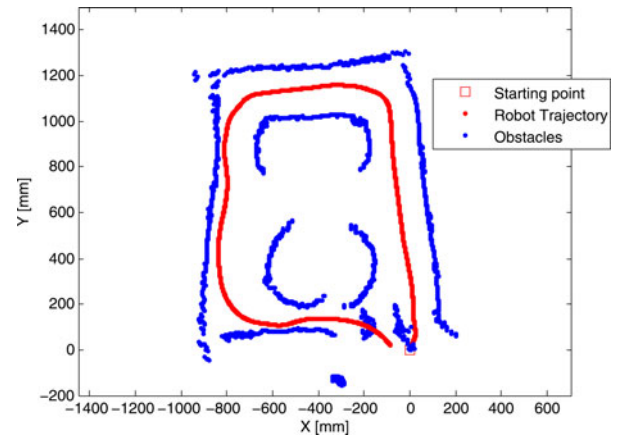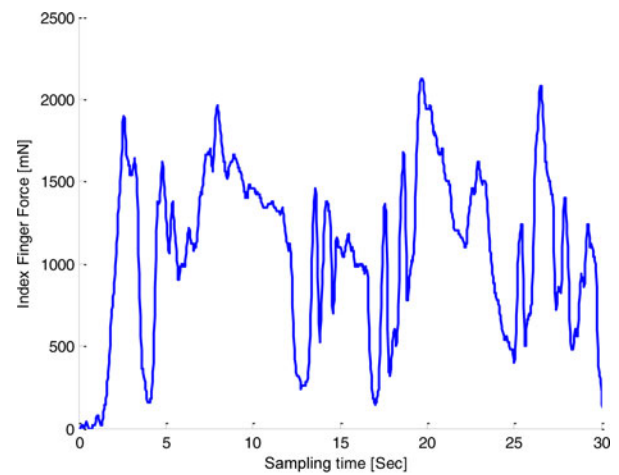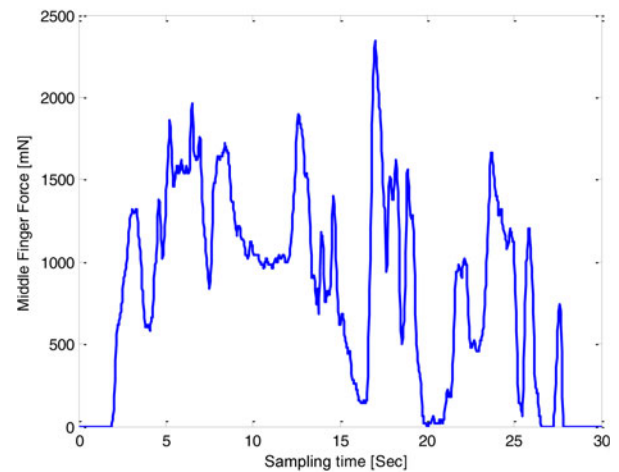
force value on the user's two finger tips during the experiment. When the robot passed the object on the left side, the force applied on the middle finger of the user dropped as shown in Fig. 20(b), specifically at about 10th, 15th, and 25th second for the three left turns. Thus, the operator knew the right time to turn and avoided collision. Similarly, when the robot got close to

the wall on the right side, the force applied on the index finger increased and made the user to turn the robot left, at about 20th and 27th second [Fig. 20(a)]. The mapping in Fig. 19 also demonstrated this procedure.

A video of the experiment can be found in this link: www.seas.gwu.edu/~bentzvi/HAPTICS/HapticGlove.html.

VI. Discussion and Future Work

This paper presented the design and experimental evaluation of a new haptic glove mechanism. Based on the performance requirements outlined in Section I, the main contributions and novelty of this paper are summarized as follows.

1) Size and Weight—The whole system, including the glove skeleton and mechanism, battery, actuator unit, control system, and wireless module, weighs only 180 g. Besides being lightweight, it is also a portable, wireless, and self-contained actuator system. In addition, the proposed glove uses PCBs to reduce the weight of the mechatronic system. The custom-made PCBs not only work as electrical component carriers and connections, but also serve as the mechanism links. On each finger, three hall-effect rotational sensors provide accurate joint angle data to calculate the finger position. One force sensor and shunt circuit for measuring the motor current were also adopted. Thus, three joint angles and torque/force measurements are available in a highly compact package for feedback control and for data collection with no need for additional glove or measurement equipment.

2) *Flexibility of Mechanism*—The glove is also flexible in its ability to accommodate different sizes and shapes of anthropomorphic fingers without constraining the natural movement of the hand. The three joints of each link are driven by a single actuator unit through a uniquely designed push–pull cable mechanism.

3) *Dynamic Range*—A compact embedded worm-gear mechanism was adopted to provide force feedback from near zero to 35 N at each fingertip. Due to the nonbackdrivability of the worm-gear mechanism, high force feedback is obtained and lower electrical power consumption is achieved through the force control algorithm.

The performance of the haptic glove was evaluated on a mobile robot in a master–slave control experiment with force feedback. Because of the integrated force feedback, the operator can "feel" what the robot senses (e.g., distance to an obstacle), which enables a smoother and safer human-in-the-loop control of the robot. By comparing the two kinds of teleoperation with and without force feedback, the experimental results show that this new admittance glove with force feedback can augment telepresence.

Compared to the PHANTOM and force-feedback joysticks [7]–[9] in mobile robot teleoperation, the proposed glove mechanism has the following advantages:

1) Since fingers are far more dexterous than the wrist, data gloves provide accurate motion capture [37]. Since the human hand has large information capacity in gesture-based communication [38], the glove mechanism can pro-

vide rich vocabulary while being intuitive to users [39]. These features make hand gestures an attractive tool to interact with robots [31]. Hand gestures have also been considered to create interface devices that may replace the conventional joystick with improved naturalness and portability [40], [41].

2) Since wireless glove apparatus is a valuable communication method, it makes controlling robots during covert or hazardous missions possible [42]. Besides, the glove does not require the operator to keep in touch with the controller module. The user may move during control operation, and therefore, can operate the robot in various situations and positions. For example, the user can lie prone to maintain covertness, which offers a low-profile advantage on the battlefield [42].

3) The glove is a self-contained haptic system which does not require external additional devices such as computer to read and process data, but for both PHANTOM and a joystick controller, this is necessary [6]–[9].

In the future, the two-finger design will be further developed into a five-finger design. This system will employ all anthropomorphic fingers with sufficient dexterity to control the navigation and manipulation of the Hybrid Mobile Robot in our lab [43]–[45]. Other application including medical training and rehabilitation therapy will be considered for our glove system.

References

[1] V. Hayward, O. Astley, M. Cruz-Hernandez, D. Grant, and G. Robles-De-La-Torre, "Haptic interfaces and devices," *Sensor Rev.*, vol. 24, pp. 16–29, Nov. 2004.

[2] T. Coles, D. Melange, and N. John, "The role of haptic in medical training simulators: A survey of the state of the art," *IEEE Trans. Haptics*, vol. 4, no. 1, pp. 51–66, Jan./Feb. 2011.

[3] M. Ferre, I. Galiana, R. Wirz, and N. Tuttle, "Haptic device for capturing and simulating hand manipulation rehabilitation," *IEEE/ASME Trans. Mechatronics*, vol. 16, no. 5, pp. 808–815, Oct. 2011.

[4] F. Gosselin, C. Bidard, and J. Brisset, "Design of a high fidelity haptic device for telesurgery," in *Proc. IEEE Int. Conf. Robot. Autom.*, Apr. 18–22, 2005, pp. 205–210.

[5] X. Wang and P. X. Liu, "Improvement of haptic feedback fidelity for telesurgical applications," *Electron. Lett.*, vol. 42, no. 6, pp. 327–329, 2006.

[6] S. Lee, G. S. Sukhatme, G. J. Kim, and C.-M. Park, "Haptic control of a mobile robot: A user study," presented at the IEEE/RSJ Int. Conf. Intelligent Robots and Systems, Lausanne, Switzerland, Oct. 2002.

[7] S. K. Cho, H. Z. Jin, J. Lee, and B. Yao, "Teleoperation of a mobile robot using a force-reflection joystick with sensing mechanism of rotating magnetic field," *IEEE/ASME Trans. Mechatronics*, vol. 15, no. 1, pp. 17–26, Feb. 2010.

[8] L. M. Crespo and D. J. Reinkensmeyer, "Haptic guidance can enhance motor learning of a steering task," *J. Motor Behavior*, vol. 40, no. 6, pp. 545–556, 2008.

[9] X. Chen and S. Agrawal, "Assisting versus repelling force-feedback for learning of a line following task in a wheelchair," *IEEE Trans. Neural Syst. Rehabil. Eng.*, vol. 21, no. 6, pp. 959–968, Nov. 2013.

[10] Z. Ni, A. Bolopion, J. Agnus, R. Benosman, and S. Regnier, "Asynchronous event-based visual shape tracking for stable haptic feedback in microrobotics," *IEEE Trans. Robot.*, vol. 28, no. 5, pp. 1081–1089, Oct. 2012.

[11] A. Bolopion and S. Regnier, "A review of haptic feedback teleoperation systems for micromanipulation and microassembly," *IEEE Trans. Autom. Sci. Eng.*, vol. 10, no. 3, pp. 496–502, Jul. 2013.

[12] S. D. Lay and A. M. Day, "Recent developments and applications of haptic devices," *Comput. Graph. Forum*, vol. 22, no. 2, pp. 117–132, 2003.

[13] PHANTOM. (Sep. 2002). [Online]. Available: http://www.sensable.com/haptic-phantom-desktop.htm

[14] M. Turner, D. Gomez, M. Tremblay, and M. Cutkosky, "Preliminary tests of an arm-grounded haptic feedback device in telemanipulation," in *Proc. ASME Dyn. Syst. Control Div.*, 1998, vol. DSC-64, pp. 145–149.

[15] CyberGrasp. (Dec. 1999). [Online]. Available: http://www.vrlogic.com/index.php/en/datagloves/cyberglovesystems.

[16] J. Blake and H. B. Gurocak, "Haptic glove with MR brakes for virtual reality," *IEEE/ASME Trans. Mechatronics*, vol. 14, no. 5, pp. 606–615, Oct. 2009.

[17] M. Bouzit, G. Burbea, G. Popescu, and R. Boian, "The Rutgers master II-New design force-feedback glove," *IEEE/ASME Trans. Mechatronics*, vol. 7, no. 2, pp. 256–263, Jun. 2002.

[18] S. Winter and M. Bouzit, "Use of magnethorheological fluid in a force feedback glove," *IEEE Trans. Neural Syst. Rehabil. Eng.*, vol. 15, no. 1, pp. 2–8, Mar. 2007.

[19] Y. Fu, P. Wang, S. Wang, H. Liu, and F. Zhang, "Design and development of a portable exoskeleton based CPM machine for rehabilitation of hand injuries," in *Proc. IEEE Int. Conf. Robot. Biomimetics*, Dec. 2007, pp. 1476–1481.

[20] F. Kobayashi, G. Ikai, W. Fukui, and F. Kojima, "Two-Fingered haptic device for robot hand teleoperation," *J. Robot.*, vol. 2011, article 419465, 2011.

[21] E. B. Brokaw, I. Black, R. J. Holly, and P. S. Lum, "Hand spring operated movement enhancer (HandSOME): A portable, passive hand exoskeleton for stroke rehabilitation," *IEEE Trans. Neural Syst. Rehabil. Eng.*, vol. 19, no. 4, pp. 391–399, Aug. 2011.

[22] S. Nakagawara, H. Kajimoto, N. Kawakami, and S. Tachi, "An encounter-type multi-fingered master hand using circuitous joints," in *Proc. IEEE Int. Conf. Robot. Autom.*, 2005, pp. 2667–2672.

[23] J. Iqbal, N. Tsagarakis, and D. Caldwell, "Design of a wearable direct-driven optimized hand exoskeleton device," in *Proc. Int. Conf. Adv. Comput.-Human Interactions*, 2011, pp. 142–146.

[24] Z. MA and P. Ben-Tzvi, "An admittance-type haptic device-RML glove," presented at the ASME Int. Mechanical Eng. Congress Exposition, Denver, CO, USA, Nov. 11–17, 2011.

[25] MABUCHI Motor, (2003, Nov.). [Online]. Available: http://www.pololu.com/file/download/fa_130ra.pdf?file_id = 0J11.

[26] Arm, Hand, and Thumb/Finger Strength. (2008). [Online]. Available: http://msis.jsc.nasa.gov/sections/section04.htm#Figure%204.9.3–4.

[27] J. Biggs and M. A. Srinivasan, "Tangential versus normal displacements of skin: relative effectiveness for producing tactile sensations," in *Proc. 10th Symp. Haptic Interfaces Virtual Environ. Teleoperator Syst.*, Orlando, FL, USA, 2002, pp. 121–128.

[28] B. Siciliano and O. Khatib, *Handbook of Robotics*. New York, NY, USA: Springer, 2008, p. 720.

[29] Ultrasonic Sensors (SRF08 and SRF02). (2008 Jan.). [Online]. Available: http://www.robot-electronics.co.uk/.

[30] Moezzi and R. Jain, "ROBOGEST: Telepresence using hand gestures," Tech. Rep. VCL-94-104, Univ. of California, San Diego, CA, USA, 1994.

[31] S. Iba, W. J. M. Vande, C. J. J. Paredis, and P. K. Khosla, "An architecture for gesture-based control of mobile robots," in *Proc. IEEE/RSJ Int. Conf. Intell. Robots Syst.*, Oct. 1999, vol. 2, pp. 851–857.

[32] J. Wachs, U. Kartoun, H. Stern, and Y. Edan, "Real-time hand gesture telerobotic system using fuzzy c-means clustering," in *Proc. Fifth Biannu. World Autom. Congr.*, Jun. 2002, pp. 403–409.

[33] W. D. Potter, L. Deligiannidis, B. J. Wimpey, H. Uchiyama, R. Deng, S. Radhakrishnan, and D. H. Barnhard, "HelpStar technology for semi-autonomous wheelchairs," presented at the Int. Conf. Computers People Special Needs, Las Vegas, NV, USA, Jun. 2005.

[34] R. F. F. Weir, "Design of artificial arms and hands for prosthetic applications," *Standard Handbook of Biomedical Engineering and Design*, New York, NY, USA: McGraw-Hill, 2003, pp. 32.1–32.61.

[35] T. W. Fong, C. Thorpe, and C. Baur, "Advanced interfaces for vehicle teleoperation: Collaborative control, sensor fusion displays, and webbased tools," *Auton. Robots*, vol. 11, no. 1, pp. 77–85, Jul. 2001.

[36] O. Linda and M. Manic, "Self-organizing fuzzy haptic teleoperation of mobile robot using sparse sonar data," *IEEE Trans. Ind. Electron.*, vol. 58, no. 8, pp. 3187–3195, Aug. 2011.

[37] A. Uribe, B. Perez-Gutierrez, and S. Alves, "Gesture-based teleoperation using a holonomic robot," in *Proc. 12th Int. Conf. Control, Autom. Syst.*, Oct. 2012, pp. 208–213.

[38] M. Zhi-Hong, L. Heung-No, R. J. Sclabassi, and S. Mingui, "Information capacity of the thumb and the index finger in communication," *IEEE Trans. Biomed. Eng.*, vol. 56, no. 5, pp. 1535–1545, May 2009.

[39] N. X. Tran, H. Phan, V. V. Dinh, J. Ellen, B. Berg, J. Lum, E. Alcantara, M. Bruch, M. G. Ceruti, C. Kao, D. Garcia, S. Fugate, and L. Duffy, "Wireless data glove for gesture-based robotic control," in *Proc. Int. Conf. Human-Comput. Interaction (HCI)*, Jul. 2009, vol. 5611, pp. 271–280.

[40] V. I. Pavlovic, R. Sharma, and T. S. Huang, "Visual interpretation of hand gestures for human–computer interaction: A review," *IEEE Trans. Pattern Anal. Mach. Intell.*, vol. 19, no. 7, pp. 677–695, Jul. 1997.

[41] L. Dipietro, A. M. Sabatini, and P. Dario, "A survey of glove-based systems and their applications," *IEEE Trans. Syst., Man, Cybern. C*, vol. 38, no. 4, pp. 461–482, 2008.

[42] M. G. Ceruti, V. V. Dinh, N. X. Tran, H. V. Phan, L. T. Duffy, T. A. Ton, G. Leonard, E. W. Medina, O. Amezcua, S. Fugate, G. Rogers, R. Luna, and J. Ellen, "Wireless communication glove apparatus for motion tracking, gesture recognition, data transmission, and reception in extreme environments," in *Proc. 24th ACM Symp. Appl. Comput.*, Mar. 2009, pp. 172–176.

[43] P. Ben-Tzvi, A. A. Goldenberg, and J. W. Zu, "Design and analysis of a hybrid mobile robot mechanism with compounded locomotion and manipulation capability," *Trans. ASME, J. Mech. Des.*, vol. 130, no. 7, pp. 1–13, Jul. 2008.

[44] P. Ben-Tzvi, "Experimental validation and field performance metrics of a hybrid mobile robot mechanism," *J. Field Robot.*, vol. 27, no. 3, pp. 250–267, May 2010.

[45] P. Ben-Tzvi, S. Ito, and A. A. Goldenberg, "A mobile robot with autonomous climbing and descending of stairs," *Robot. J.*, vol. 27, no. 2, pp. 171–188, Feb. 2009.
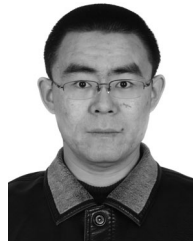
Zhou Ma (S'10) received the Master's degree in electrical engineering from the University of Science and Technology, Beijing, China, in 2009, with a thesis focused on small-scale humanoid robots. He is currently working toward the Ph.D. degree at the Robotics and Mechatronics Laboratory, Department of Mechanical and Aerospace Engineering, The George Washington University, Washington, DC, USA.

His current research interests include basic and applied research in robotics and mechatronics, and involve investigations in haptics glove design, simulation, optimization, and integration, with applications to teleoperation, virtual reality, and rehabilitation.

Pinhas Ben-Tzvi (S'02–M'08–SM'12) received the B.S. degree (*summa cum laude*) in mechanical engineering from the Technion—Israel Institute of Technology, Haifa, Israel, in 2000 and the M.S. and Ph.D. degrees in mechanical engineering from the University of Toronto, Toronto, ON, Canada, in 2004 and 2008, respectively.

He is currently an Assistant Professor in the Department of Mechanical and Aerospace Engineering and the Founding Director of the Robotics and Mechatronics Laboratory at The George Washington University, Washington, DC, USA. Before joining the University of Toronto in 2002, he was an R&D Engineer with General Electric Medical Systems Company, developing medical diagnostic robotic and mechatronic systems. His current research interests include robotics and autonomous systems, mechatronics, dynamic systems and control, mechanism/machine design and integration, and sensing and actuation. Applications include robust dynamic stabilization and agile maneuvering of mobile robots using intelligent biomimetic robotic tails; autonomous mobile robot mobility and manipulation and modular and reconfigurable mobile robotics for search and rescue, environment monitoring, and defense; advanced devices and robotic systems for medicine; haptics devices and exoskeletons for robot control and rehabilitation; and novel sensors and actuators for biomedical applications. He has authored or coauthored more than 60 peer-reviewed journal articles and refereed papers in conference proceedings and is the inventor of five U.S. patents and a Canadian patent.

Dr. Ben-Tzvi received the 2013 GW SEAS Outstanding Young Researcher Award and the GW SEAS Outstanding Young Teacher Award, as well as several other honors and awards. He is a member of the American Society of Mechanical Engineers (ASME).